Supporting Information

$REV_3(BO_3)_4$ (RE = La–Nd): A Series of Rare Earth Vanadoborates Exhibit Large Birefringence Induced by Distorted $V^{III}O_6$ Groups

Yu-Long Wei[+], *Wen-Dong Yao*[+], *Yi-Lei Lv, Liang Ma, and Ru-Ling Tang**

School of Chemistry and materials, Yangzhou University, Yangzhou, Jiangsu 225002, P. R. China. E-mail: rltang@yzu.edu.cn

[+] *These authors contributed equally to this work.*

Corresponding author: rltang@yzu.edu.cn

Contents

Experimental Section

Syntheses and analyses.

All starting materials were used as received without further purification. Single crystals of **1**–**4** were obtained by solid–state reactions. 500 mg mixture of La_2O_3 (99.99 %) / CeO_2 (99.99 %) / Pr_2O_3 (99.99 %) / Nd_2O_3 (99.99 %), V_2O_3 (99.9 %) and B_2O_3 (99.9 %) with RE_2O_3 : V_2O_3 : B_2O_3 molar ratios of 1 : 3 : 4, as well as 400 mg KI (99 %) as flux were used as raw materials. The starting materials were adequately ground into powder in agate mortar, pressed into pellets, and loaded into quartz tubes. The tubes were evacuated to 1×10^{-4} torr and flame-sealed. The samples were placed into a muffle furnace, heated from room temperature to 950 °C, and subsequently cooled to 300 °C with a rate of 3 °C/h, and finally powered off. Crystals of **1**–**4** were obtained after washed with deionized water and ethyl alcohol. Crystals retained their morphology after storage in air at room temperature for over six months. Furthermore, their tolerance to common polar solvents was confirmed, as all samples were washed with deionized water and ethanol after synthesis without observable degradation prior to characterization. Unfortunately, the yields of compounds **1**–**4** were generally low, which, based on our observations and synthetic attempts, can be reasonably attributed to the complexity of the quaternary RE_2O_3–V_2O_3–B_2O_3 system, which is thermodynamically favorable for the formation of competing binary or ternary phases (e.g., $REBO_3$). Furthermore, the tendency of boron-containing systems to form amorphous borates, and the narrow synthetic window required for the crystallization of the target vanadium borate phase, further limited the achievable yields.

A semiquantitative elemental analysis was performed on several single crystals of **1**–**4** using a field-emission scanning electron microscope (FE-SEM, Zeiss, Supra55) equipped with an energy dispersive X-ray spectroscope (EDS, Bruker, Quantax), which confirms the existence of La / Ce / Pr / Nd, V and O elements (Fig. S2) and atom ratios are close to the crystal structure determination results (Table S3).

The powder X-ray diffraction (PXRD) patterns were collected with a Bruker D8 Advance diffractometer at 40 kV and 100 mA for Cu–Kα radiation (λ = 1.5406 Å) with a scan speed of 5°/min at room temperature. The simulated patterns were generated with the Mercury v3.8 program provided by the CCDC and single-crystal reflection data. As shown in Fig. S3, the experimental PXRD patterns, as well as those measured after six months, both align well with the corresponding simulated pattern, indicating high purity of the synthesized samples.

Crystal Data.

The crystallography data of **1**–**4** were collected on a Bruker D8 QUEST X–ray diffractometer with graphite–monochromated Mo–Kα radiation (λ = 0.71073 Å). The structures were solved by Direct Methods and refined by full–matrix least–squares techniques on F^2 with anisotropic displacement parameters for all atoms using SHELX–2014.[1] All of the processes were performed within Olex2.[2] The final refinements included anisotropic displacement parameters for all atoms and a secondary extinction correction. The crystallographic data and bond lengths are summarized in Tables 1 and S1, respectively.

UV–Vis–NIR diffuse-reflectance spectra.

The diffuse reflectance data were collected with a Varian Cary 5000 UV–Vis–NIR spectrometer in the wavelength range of 200–1200 nm at room temperature. The optical energy gaps of **1** and **4** were measured with pure samples. The absorption spectra were calculated from the reflection spectra by the Kubelka–Munk function,[3-4] and Tauc plot was used to calculate the band gap.[5]

IR spectra.

The IR and Raman spectra of **1** and **4** were measured using a Magna 750 FT-IR spectrometer with KBr as the background in a range 4000–400 cm^{-1} with a resolution of 2 cm^{-1} and A DXR2xi Micro Raman Imaging Spectrometer under the range of 200–2000 cm^{-1}, respectively.

Thermal behaviours.

Thermogravimetric analysis (TG) and differential scanning calorimeter (DSC) measurements on powder samples of **1** and **4** were carried out on the NETZSCH STA449C unit, with a heating rate of 10 °C min^{-1} from 20 to 1000 °C in nitrogen.

Magnetic susceptibility measurements.

Temperature-dependent magnetic susceptibilities of **1** and **4** were measured by a Quantum Design PPMS from 2 to 300 K in an applied magnetic field of 1000 Oe. The polycrystalline powdery samples were secured in gel capsules.

Birefringence measurements.

The birefringence was assessed with a polarizing microscope (NIKON Eclipse Ci-POL) equipped with a quartz wedge compensator under the light source of 546 nm. According to the equation, R (retardation) = Δn × d, the birefringence was calculated, where R, Δn, and d represent the optical path difference, birefringence, and the thickness of crystal, respectively. The thickness of the crystalline sample was measured on a single-crystal XRD diffractometer.

Calculation details.

The theoretical calculations of band structure, density of states (DOS), and birefringence of **1**, $LaSc_3(BO_3)_4$ (*C*2/*c*), $LaSc_3(BO_3)_4$ (*Cc*), $LaSc_3(BO_3)_4$ (*R*32), and $GdAl_3(BO_3)_4$ (*C*2) were performed by employing the CASTEP 23.1 package.[6] The generalized gradient approximation (GGA) was adopted and the Perdew-Burke-Ernzerhof (PBE) was chosen as the exchange–correlation function.[7] The employed on-the-fly generated norm-conserving pseudopotentials[8] of La, Gd, Sc, Al, V, B and O treat 4f, 5s, 5p, 5d, 6s; 4f, 5s, 5p, 5d, 6s; 3s, 3p, 3d, 4s; 3s, 3p; 3s, 3p, 3d, 4s; 2s, 2p and 2s, 2p as the valence states, respectively. The plane wave cutoff energy for the expansion of wave functions was set at 1170 eV, 1020 eV, 1020 eV, 1020 eV, 1020 eV and the tetrahedron method was used for integrations. The numerical integrations in the Brillouin zones were performed by utilizing 3 × 3 × 2, 3 × 3 × 2, 3 × 3 × 2, 3 × 3 × 4, 3 × 3 × 2 Monkhorst-Pack k-point mesh, respectively, which showed an excellent convergence of the energy differences (5×10^{-7} eV/atom), and the Fermi level (E_f = 0 eV) was chosen as the reference. DFT+U method was employed to deal with the strong correlation effects, where the U_{eff} value of V, Gd were 2.5 eV and 6 eV, respectively. The optical property was calculated and described based on the complex dielectric function $\varepsilon(\omega) = \varepsilon_1(\omega) + i\varepsilon_2(\omega)$, in which $\varepsilon_1(\omega)$ and $\varepsilon_2(\omega)$ denote the real and imaginary parts of the dielectric function, respectively.[9] Refractive index *n* was calculated based on the followed formula.

$$\varepsilon_1(\omega) = 1 + \frac{2}{\pi} p \int_0^{\infty} \frac{\omega' \varepsilon_2(\omega')}{\omega'^2 - \omega^2} d\omega'$$

$$\varepsilon_2(\omega) = \frac{2e^2\pi}{\Omega\varepsilon_0} \sum_{K,V,C} \left| \langle \psi_K^C | \hat{u} \cdot r | \psi_K^V \rangle \right|^2 \delta\left(E_K^C - E_K^V - E\right)$$

$$n(\omega) = \sqrt{\frac{\varepsilon_1^2(\omega) + \varepsilon_2^2(\omega) + \varepsilon_1(\omega)}{2}}$$

Table S1. Crystal data and structure refinement parameters for **1**–**4**.

Chemical formula	**$LaV_3(BO_3)_4$ (1)**	**$CeV_3(BO_3)_4$ (2)**	**$PrV_3(BO_3)_4$ (3)**	**$NdV_3(BO_3)_4$ (4)**
Fw	526.97	528.18	528.97	532.3
T (K)	298			
Crystal system	Monoclinic			
Space group	*C*2/*c*			
Z	4			
a (Å)	7.5691(8)	7.5498(5)	7.5419(9)	7.5261(4)
b (Å)	9.6753(9)	9.6596(6)	9.6567(13)	9.6411(5)
c (Å)	11.6060(14)	11.5824(9)	11.5679(14)	11.5559(7)
β (°)	104.937(4)	104.918(2)	104.864(4)	104.807(2)
V (Å^3)	821.23(15)	816.21(10)	814.30(18)	810.65(8)
D_{calcd} (g cm^{-3})	4.262	4.298	4.315	4.361
μ (mm^{-1})	8.483	8.878	9.292	9.729
F(000)	968	972	976	980
2θ range (°)	6.984 to 55.006	7 to 54.95	7.004 to 54.994	7.016 to 55.054
Measd. reflns	2956	4038	4851	6075
Indep. reflns/R_{int}/ R_{sigma}	0.0247/0.0289	0.0459/0.0408	0.0417/0.0291	0.0414/0.0293
R1, wR2 ($I > 2\sigma(I)$)[a]	0.0171,0.0379	0.0242,0.0425	0.0205,0.0373	0.0221,0.0410
R1, wR2 (all data)[a]	0.0194,0.0383	0.0306,0.0439	0.0244,0.0381	0.0277,0.0423
GOF on F^2	1.111	1.057	1.07	1.064
$\Delta\rho_{max}/\Delta\rho_{min,}$ e/Å^3	0.58/-0.59	1.13/-0.70	1.22/-0.58	1.56/-0.72

[a] $R1 = ||F_o| - |F_c||/|F_o|$; $wR2 = [w(F_o^2 - F_c^2)^2]/[w(F_o^2)^2]^{1/2}$.

Table S2. Important bond lengths (Å) and bond angles (°) for **1**–**4**.

Bond	Distance/Å	Bond	Angle/Å
		1	
La(1)−O(3)	2.436(2)	O(4)–La(1)–O(5)	73.62(7)
La(1)−O(4)#2	2.466(2)	O(1)–V(1)–O(1)	79.82(9)
La(1)−O(5)#4	2.477(2)	O(1)–V(1)–O(2)	93.87(9)
V(1)−O(1)#7	2.017(2)	V(1)–O(1)–V(1)	100.18(9)
V(2)−O(3)#7	1.978(2)	V(1)–O(7)–V(2)	100.35(9)
V(1)−O(7)#6	2.029(2)	B(1)–O(1)–La(2)	104.43(19)
O(5)−B(2)	1.366(4)	B(2)–O(1)–V(1)	126.86(19)
O(2)−B(2)	1.356(4)		
O(6)−B(1)	1.372(4)		
		2	
Ce(1)−O(3)#1	2.445(3)	O(4)–Ce(1)–O(5)	73.49(9)
Ce(1)−O(4)	2.424(3)	O(1)–V(1)–O(1)	79.36(12)
Ce(1)−O(5)#4	2.448(2)	O(1)–V(1)–O(2)	94.09(11)
V(1)−O(1)#7	2.010(3)	V(1)–O(1)–V(1)	100.64(12)
V(2)−O(4)	1.979(3)	V(1)–O(7)–V(2)	100.79(12)
V(1)−O(6)#6	2.023(3)	B(1)–O(1)–Ce(2)	105.4(2)
O(5)−B(2)	1.367(5)	B(2)–O(1)–V(1)	126.4(2)
O(2)−B(2)	1.366(5)		
O(6)−B(1)	1.385(5)		
		3	
Pr(1)−O(3)#1	2.432(2)	O(4)–Pr(1)–O(5)	73.47(8)
Pr(1)−O(4)	2.412(2)	O(1)–V(1)–O(1)	79.28(11)
Pr(1)−O(5)#4	2.431(2)	O(1)–V(1)–O(2)	94.14(10)
V(1)−O(1)#7	2.004(2)	V(1)–O(1)–V(1)	100.72(11)
V(2)−O(4)	1.978(2)	V(1)–O(7)–V(2)	100.83(10)
V(1)−O(6)#6	2.016(2)	B(1)–Pr(1)–B(2)	105.22(10)
O(5)−B(2)	1.369(4)	B(2)–O(1)–V(1)	126.19(19)
O(2)−B(2)	1.367(4)		

O(6)−B(1)	1.386(5)		
		4	
Nd(1)−O(3)#1	2.448(3)	O(4)–Nd(1)–O(5)	73.40(9)
Nd(1)−O(4)	2.414(2)	O(1)–V(1)–O(1)	79.18(12)
Nd(1)−O(6)#4	2.450(2)	O(1)–V(1)–O(2)	94.16(11)
V(1)−O(1)#6	2.003(3)	V(1)–O(1)–V(1)	100.82(12)
V(2)−O(4)	1.978(3)	V(1)–O(7)–V(2)	101.06(12)
V(1)−O(6)#8	1.999(3)	B(1)–Nd(1)–B(2)	105.22(12)
O(5)−B(2)	1.372(3)	B(2)–O(1)–V(1)	126.1(2)
Nd(1)−O(1)	2.3656(13)		
B(2)−O(4)	1.4791(15)		

Symmetry transformations used to generate equivalent atoms: Compound **1**: 1-*y*, +*x*-*y*, +*z*; 1-*x*, -*y*, 2-*z*; 1+*x*, +*y*, 1+*z*; +*y*, -*x*+*y*, 2-*z*; 1-*y*+*x*, +*x*, 2-*z*; -*y*+*x*, -1+*x*, 2-*z*; 1-*y*, +*x*-*y*, 1+*z*; +*x*, +*y*, 1+*z*; 1+*y*-*x*, 1-*x*, +*z*; -*x*, -*y*, 1-*z*; +*y*, -*x*+*y*, 1-*z*; -*y*, +*x*-*y*, +*z*; -*y*+*x*, +*x*, 1-*z*; +*y*-*x*, -*x*, +*z*. Compound **2**: 1-*y*, +*x*-*y*, +*z*; 1+*x*, +*y*, 1+*z*; +*y*, -*x*+*y*, 2-*z*; 1-*x*, -*y*, 2-*z*; 1-*y*+*x*, +*x*, 2-*z*; 1-*y*, +*x*-*y*, 1+*z*; +*x*, +*y*, 1+*z*; -*y*+*x*, -1+*x*, 2-*z*; 1+*y*-*x*, 1-*x*, +*z*; -*y*, +*x*-*y*, +*z*; -*y*+*x*, +*x*, 1-*z*; +*y*-*x*, -*x*, +*z*; -*x*, -*y*, 1-*z*; +*y*, -*x*+*y*, 1-*z*. Compound **3**: 1-*y*, 1+*x*-*y*, +*z*; 1-*x*, 2-*y*, 2-*z*; -1+*x*, +*y*, 1+*z*; +*y*, 1-*x*+*y*, 2-*z*; 1-*y*, 1+*x*-*y*, 1+*z*; -*y*+*x*, +*x*, 2-*z*; +*x*, +*y*, 1+*z*; 1-*y*+*x*, 1+*x*, 2-*z*; +*y*-*x*, 1-*x*, +*z*; 1+*y*-*x*, 2-*x*, +*z*; +*y*, 1-*x*+*y*, 1-*z*; 2-*y*, 1+*x*-*y*, +*z*; 2-*x*, 2-*y*, 1-*z*; 1-*y*+*x*, +*x*, 1-*z*. Compound **4**: 2-*x*, 1-*y*, 2-*z*; +*x*, -1+*y*, 1+*z*; 1+*y*-*x*, 1-*x*, 1+*z*; 1-*y*+*x*, +*x*, 2-*z*; 1+*y*, 1-*x*+*y*, 2-*z*; +*x*, +*y*, 1+*z*; +*y*, -*x*+*y*, 2-*z*; 1-*y*, +*x*-*y*, +*z*; 1+*y*-*x*, 1-*x*, +*z*; 2-*x*, 2-*y*, 1-*z*; 1-*y*+*x*, +*x*, 1-*z*; 1+*y*-*x*, 2-*x*, +*z*; +*y*, 1-*x*+*y*, 1-*z*; 2-*y*, 1+*x*-*y*, +*z*.

Table S3. Atomic coordinates (× 10^4), equivalent isotropic displacement parameters (U_{eq}[a], Å^2 × 10^3) and bond valence sums (BVS) for **1**–**4**.

Atom	*x*	*y*	*z*	U_{eq}/Å^2	BVS
			1		
La(1)	0	4634.5(3)	7500	6.92(10)	2.749
V(1)	5566.4(7)	7480.8(5)	10279.4(5)	4.66(14)	2.886
V(2)	5000	4148.0(8)	7500	5.17(17)	2.946
O(1)	2491(3)	6139(2)	4914.0(19)	6.0(5)	1.820
O(2)	3972(3)	4021(2)	5737.5(19)	6.1(5)	1.924
O(3)	3065(3)	5483(2)	7598(2)	6.9(5)	2.043
O(4)	1644(3)	7637(2)	7068(2)	7.3(5)	1.845
O(5)	4392(3)	7569(2)	8582(2)	7.5(5)	2.023
O(6)	977(3)	4028(2)	4376.8(19)	7.2(5)	1.918
B(1)	3065(5)	6869(4)	7771(3)	5.6(7)	2.959
B(2)	2496(5)	4712(4)	5027(3)	6.3(7)	2.881
			2		
Ce(1)	10000	5355.5(3)	2500	7.15(12)	2.603
V(1)	4437.8(9)	2515.5(6)	-278.8(6)	3.71(16)	2.898
V(2)	5000	5843.5(9)	2500	5.0(2)	2.950
O(1)	7502(3)	3852(3)	5079(2)	8.0(6)	1.813
O(2)	6044(3)	5981(3)	4268(2)	5.9(5)	1.950
O(3)	5612(4)	2404(3)	1425(2)	7.6(6)	1.993
O(4)	6940(4)	4508(3)	2394(2)	7.9(6)	2.003
O(5)	9030(3)	5957(3)	5635(2)	7.4(6)	1.901
O(6)	8368(4)	2356(3)	2934(2)	8.3(6)	1.863
B(1)	6944(6)	3119(5)	2225(4)	5.9(9)	2.959
B(2)	7509(5)	5291(5)	4971(3)	4.3(9)	2.901
			3		
Pr(1)	0	4646.4(3)	7500	6.33(9)	2.618
V(1)	5559.1(8)	7488.3(6)	10278.4(5)	2.09(14)	2.926

V(2)	5000	4161.9(8)	7500	2.86(18)	2.973
O(1)	2504(3)	6152(3)	4926(2)	7.9(5)	1.824
O(2)	3950(3)	4017(2)	5728(2)	5.0(5)	1.952
O(3)	4382(3)	7605(2)	8571(2)	6.2(5)	2.006
O(4)	3052(3)	5496(3)	7607(2)	6.9(5)	2.011
O(5)	961(3)	4049(3)	4356(2)	6.7(5)	1.892
O(6)	1632(3)	7651(2)	7061(2)	7.3(5)	1.877
B(1)	3056(5)	6887(4)	7775(3)	4.8(8)	2.951
B(2)	2486(5)	4714(4)	5024(3)	3.8(8)	2.882
			4		
Nd(1)	0	4644.7(3)	7500	6.13(9)	2.698
V(1)	5562.3(9)	7483.8(6)	10279.6(5)	0.72(14)	2.932
V(2)	5000	4155.9(9)	7500	1.73(18)	2.961
O(1)	2500(3)	6152(3)	4918(2)	5.1(5)	1.841
O(2)	3964(3)	4025(3)	5735(2)	3.2(5)	1.950
O(3)	4385(4)	7592(3)	8577(2)	5.2(5)	2.023
O(4)	3053(3)	5485(3)	7607(2)	4.2(5)	2.020
O(5)	1630(3)	7644(3)	7063(2)	5.7(6)	1.934
O(6)	966(3)	4040(3)	4367(2)	4.1(5)	1.874
B(1)	3063(5)	6879(4)	7777(3)	2.2(7)	2.975
B(2)	2494(5)	4711(5)	5029(3)	0.7(7)	2.906

[a] U_{eq} is defined as one third of the trace of the orthogonalized U_{ij} tensor.

Table S4. EDS quantitative analysis atom ratios in **1**–**4**.

Element	Ratio	**1** (at. %)	**2** (at. %)	**3** (at. %)	**4** (at. %)
RE	1	1.88	2.93	3.98	2.20
V	3	5.42	8.27	10.53	6.09
O	12	23.16	40.20	43.44	34.32

Table S5. The V coordination environments and anion frameworks in $NaV[BP_2O_7(OH)_3]$, $CsV_3(H_2O)_2[B_2P_4O_{16}(OH)_4]$, $AV(BP_2O_8(OH))$ (A = K, Rb and NH_4), $Li_3V_2[BP_3O_{12}(OH)][HPO_4]$, $V_2[B(PO_4)_3]$, VBO_3 and **1**.

Compound	V coordination geometry	Anion framework
$NaV[BP_2O_7(OH)_3]$	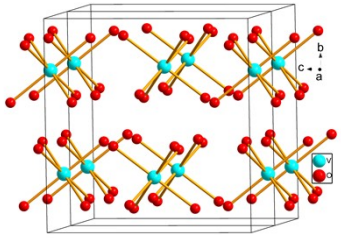	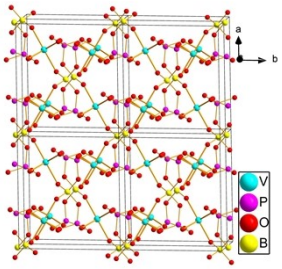
$CsV_3(H_2O)_2[B_2P_4O_{16}(OH)_4]$		
$AV(BP_2O_8(OH))$ (A = K, Rb and NH_4)	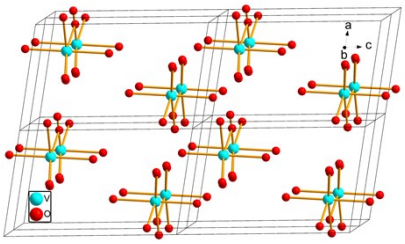	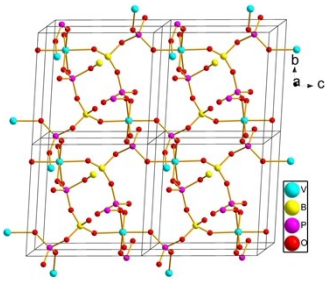
$Li_3V_2[BP_3O_{12}(OH)][HPO_4]$		
$V_2[B(PO_4)_3]$	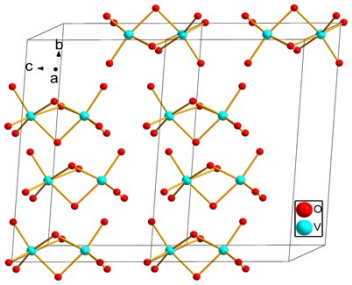	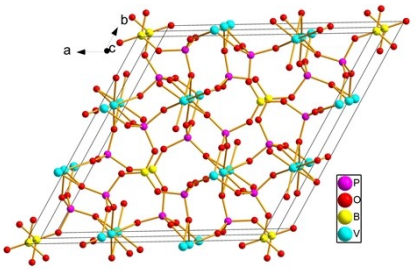
VBO_3	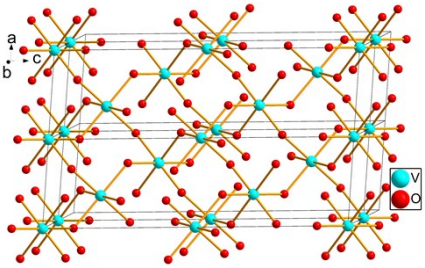	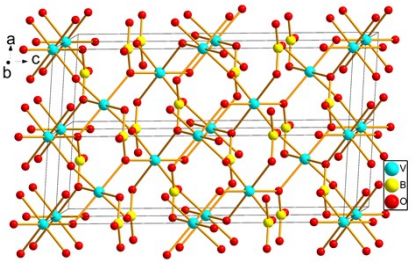
1	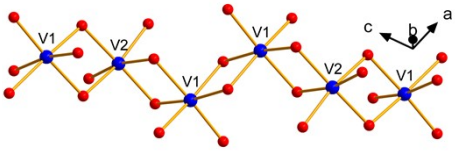	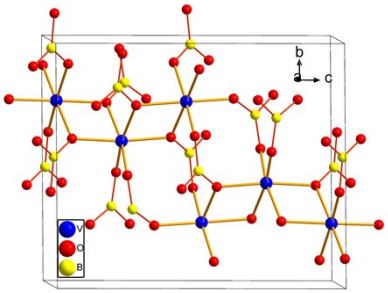

Table S6. Comparison of reported rare-earth borate birefringent crystals.

crystal	space group	Measured birefringence	Calculate birefringence
$LaBO_3$	*Pnma*	0.093@546 nm	0.110@546 nm
$K_2GdB_3O_6F_2$	*Pbcn*	0.12@589 nm	0.124@532 nm
$LiRb_2YB_2O_6$	*Pbcm*	0.039@532 nm	0.038@532 nm
$CaRbYB_2O_6$	*Pbca*	0.045@532 nm	0.048@532 nm
$Li_2RbY_4B_5O_{15}$	*P*2/*n*	0.11@532 nm	0.104@532 nm
$Li_2CsY_4B_5O_{15}$	*P*2/*n*	0.10@532 nm	0.103@532 nm
$RbBaYB_6O_{12}$	$R\bar{3}$	0.12@589 nm	0.1@589 nm
$CsBaYB_6O_{12}$	$R\bar{3}$	0.12@589 nm	0.1@589 nm
$K_2YB_3O_6F_2$	*Pbcn*	0.094@532 nm	0.101@532 nm
$Rb_2YB_3O_6F_2$	*C*2	0.081@532 nm	0.090@532 nm
$Ba_2K_{1.6}Na_{0.4}Sc_2(BO_3)_4$	$R\bar{3}m$	0.11@550 nm	0.102@550 nm
α-$Ba_3Sc_2(BO_3)_4$	$P\bar{3}c1$	0.14@550 nm	0.090@550 nm
β-$Ba_3Sc_2(BO_3)_4$	$P\bar{3}m1$	0.149@550 nm	0.096@550 nm
$RbBaScB_6O_{12}$	$R\bar{3}$	0.139@550 nm	0.0988@550 nm
$KNa_2Lu(BO_3)_2$	*Pnma*	0.0436@1064 nm	0.044@1064 nm
α-$BaGdBO_3F_2$	$P2_1/c$	0.072@546 nm	0.068@546 nm
β-$BaGdBO_3F_2$	$Cmc2_1$	0.059@546 nm	0.055@546 nm
$LaCa_4O(BO_3)_3$	*Cm*	0.036@589 nm	0.071@589 nm
$YCa_4O(BO_3)_3$	*Cm*	0.043@589 nm	0.071@589 nm
$K_2NaYB_2O_6$	$P2_1/c$	0.03@1064 nm	0.028@1064 nm
$Na_3La_9O_3(BO_3)_8$	$P\bar{6}2m$	0.090@589 nm	0.090@589 nm
$LiNa_2Y(BO_3)_2$	$P2_1/n$	0.019@532nm	0.017@532nm
$RbNa_2Y(BO_3)_2$	*Pnma*	0.031@532nm	0.033@532nm
$RbSrY(BO_3)_2$	$P2_1/m$	0.071@532nm	0.07@532nm
$LaV_3(BO_3)_4$	*C*2/*c*	0.18@546 nm	0.171@546 nm

Table S7. Calculated birefringences and band gaps in the Huntite family for four typical space groups.

Crystal	Space group	Calculated birefringence at 550 nm	Calculated birefringence at 1064 nm	Calculated band gap [eV]
$LaSc_3(BO_3)_4$	*C*2/*c*	0.071	0.064	4.482
$GdAl_3(BO_3)_4$	*C*2	0.036	0.034	4.641
$LaSc_3(BO_3)_4$	*Cc*	0.073	0.063	4.429
$LaSc_3(BO_3)_4$	*R*32	0.101	0.092	4.267

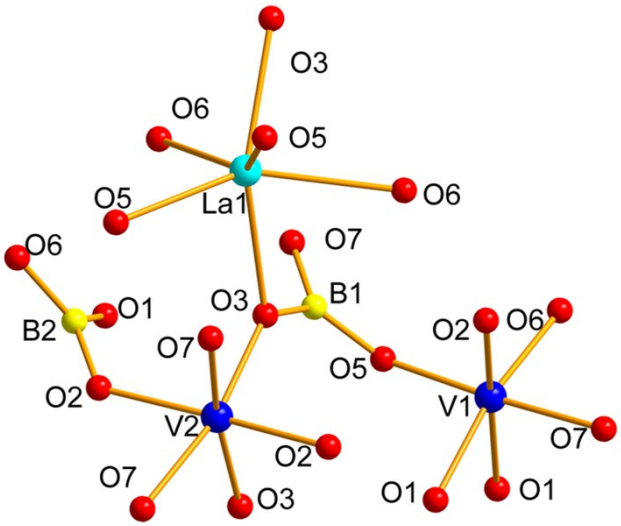

Figure S1. Coordination geometry of **1**.

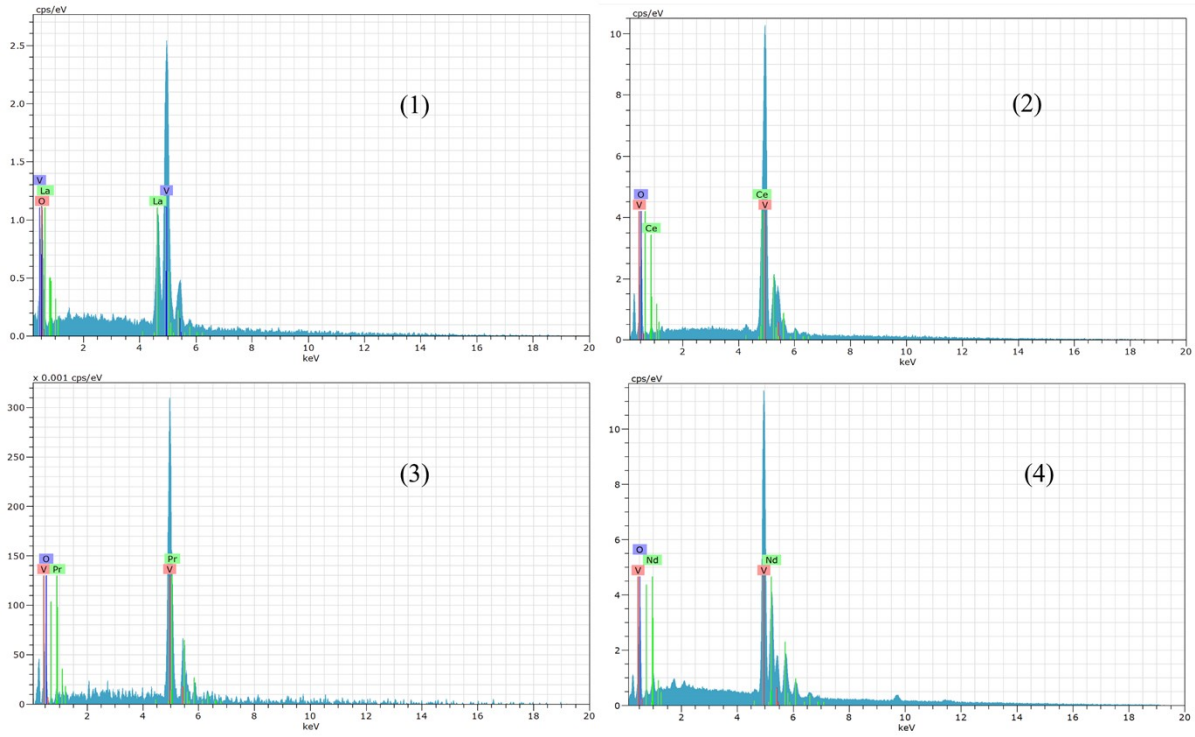

Figure S2. Energy dispersive X–ray spectroscopies of **1**–**4**.

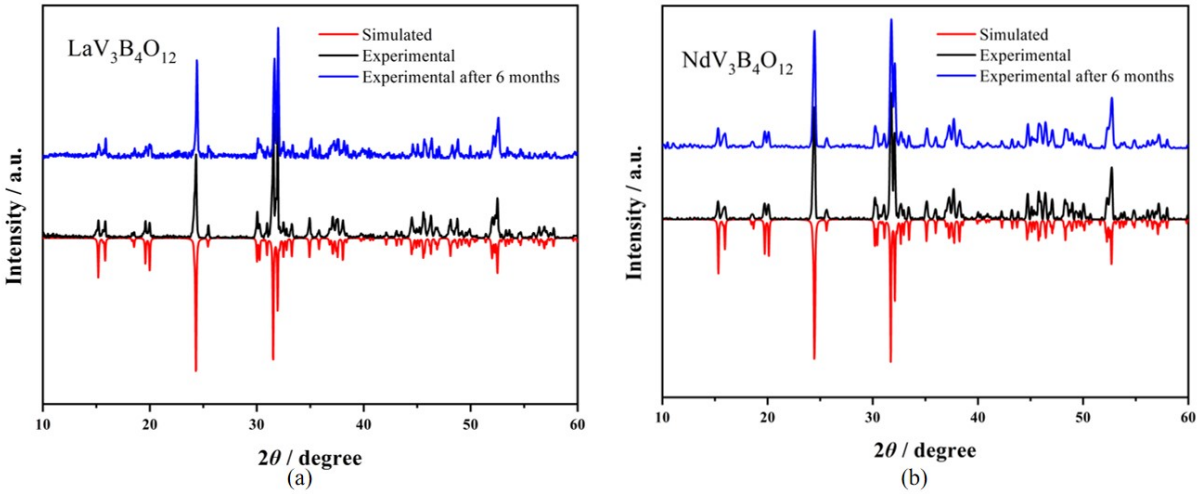

Figure S3. The PXRD patterns for **1** (a) and **4** (b).

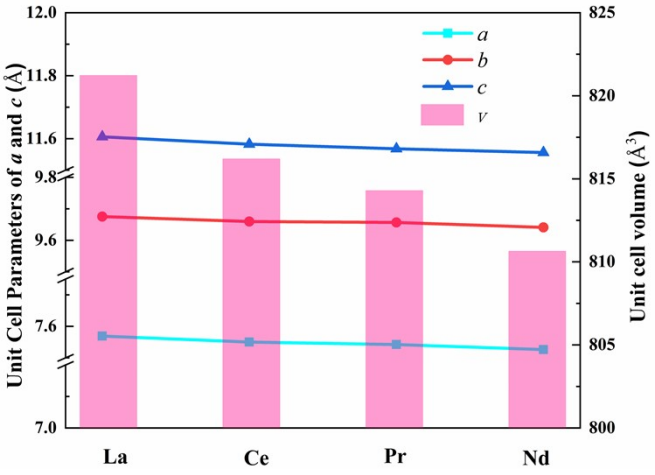

Figure S4. The unit cell parameters of *a*, *b*, *c* and *V* in **1**–**4**.

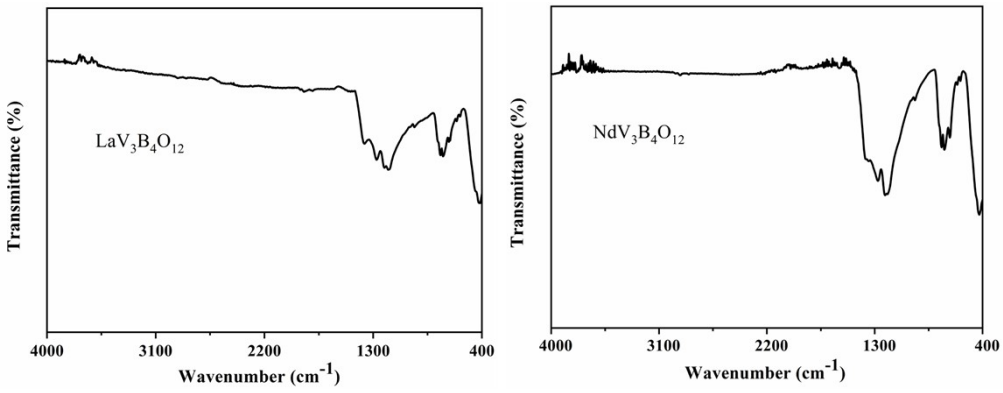

Figure S5. The IR spectra of **1** (a) and **4** (b).

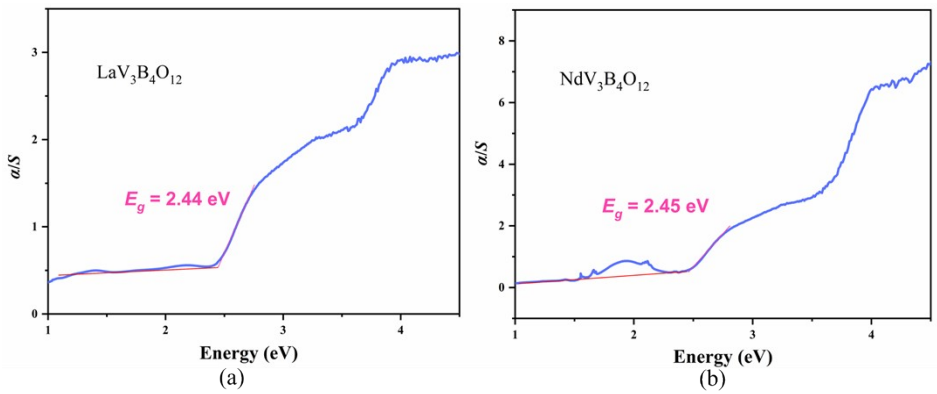

Figure S6. UV−vis−NIR diffuse reflectance spectra of **1** (a) and **4** (b).

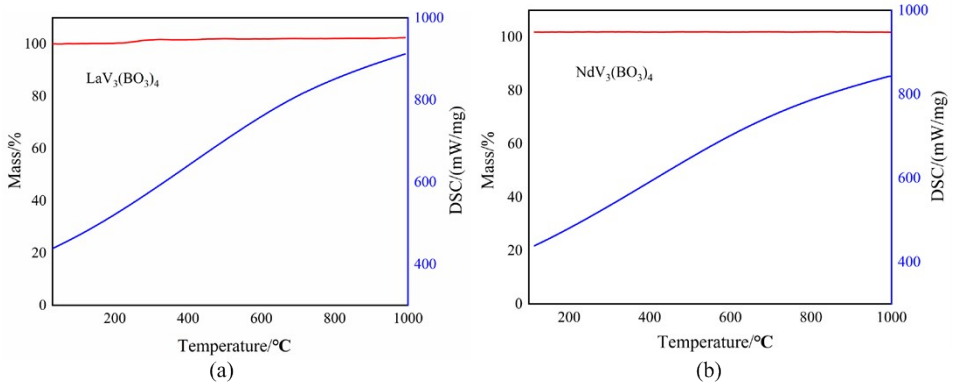

Figure S7. The TG-DSC curves of **1** (a) and **4** (b).

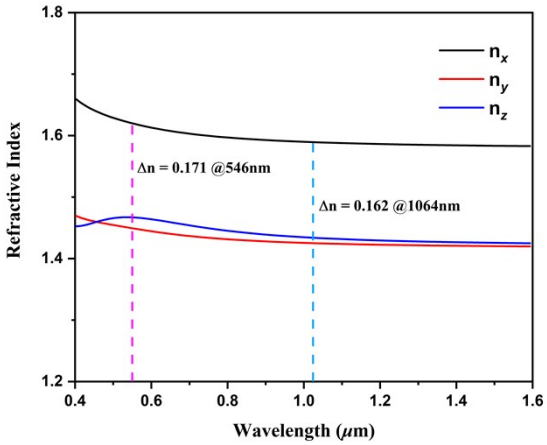

Figure S8. The calculated wavelength-dependent refractive index curves of **1**.

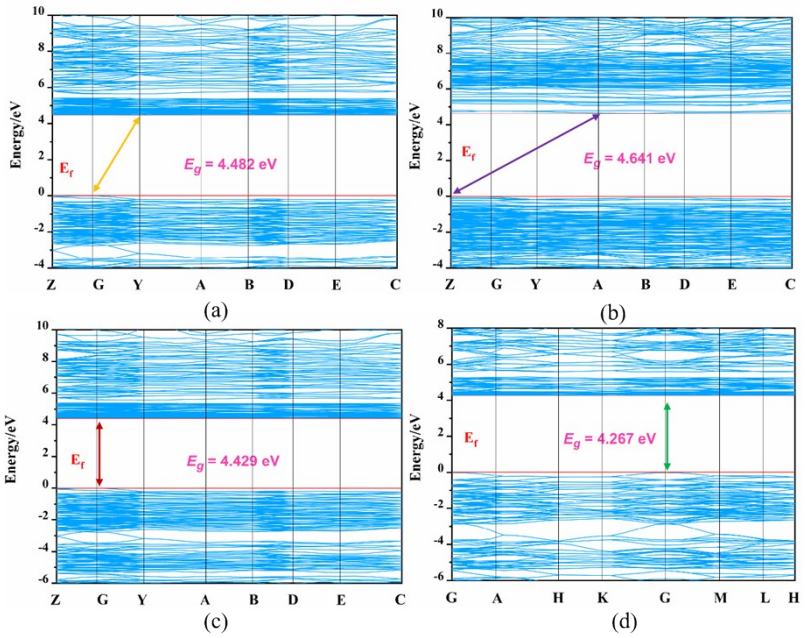

Figure S9. Calculated band structures of the huntite family members: (a) $LaSc_3(BO_3)_4$ (*C*2/*c*), (b) $GdAl_3(BO_3)_4$ (*C*2), (c) $LaSc_3(BO_3)_4$ (*Cc*) and (d) $LaSc_3(BO_3)_4$ (*R*32).

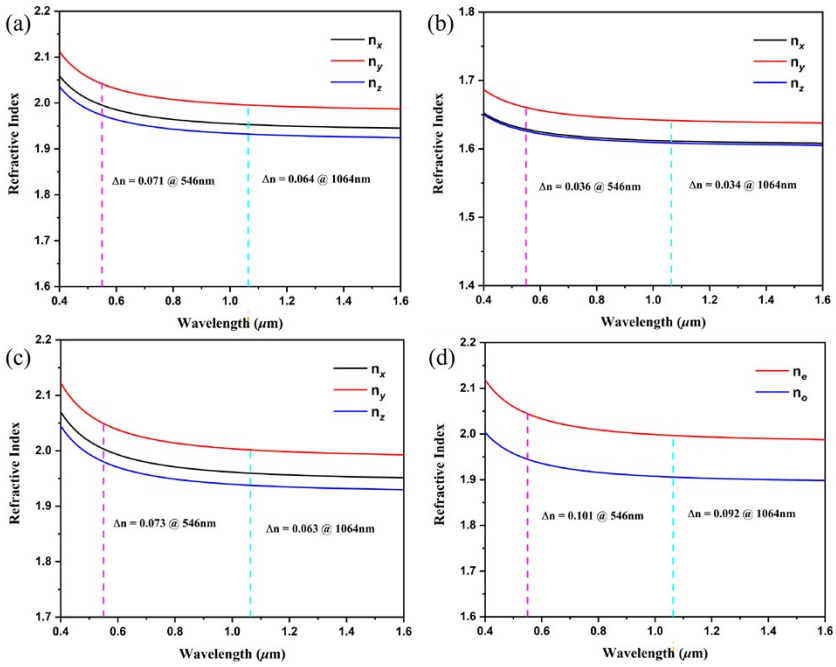

Figure S10. Calculated birefringences of the huntite family members: (a) $LaSc_3(BO_3)_4$ (*C*2/*c*), (b) $GdAl_3(BO_3)_4$ (*C*2), (c) $LaSc_3(BO_3)_4$ (*Cc*) and (d) $LaSc_3(BO_3)_4$ (*R*32).

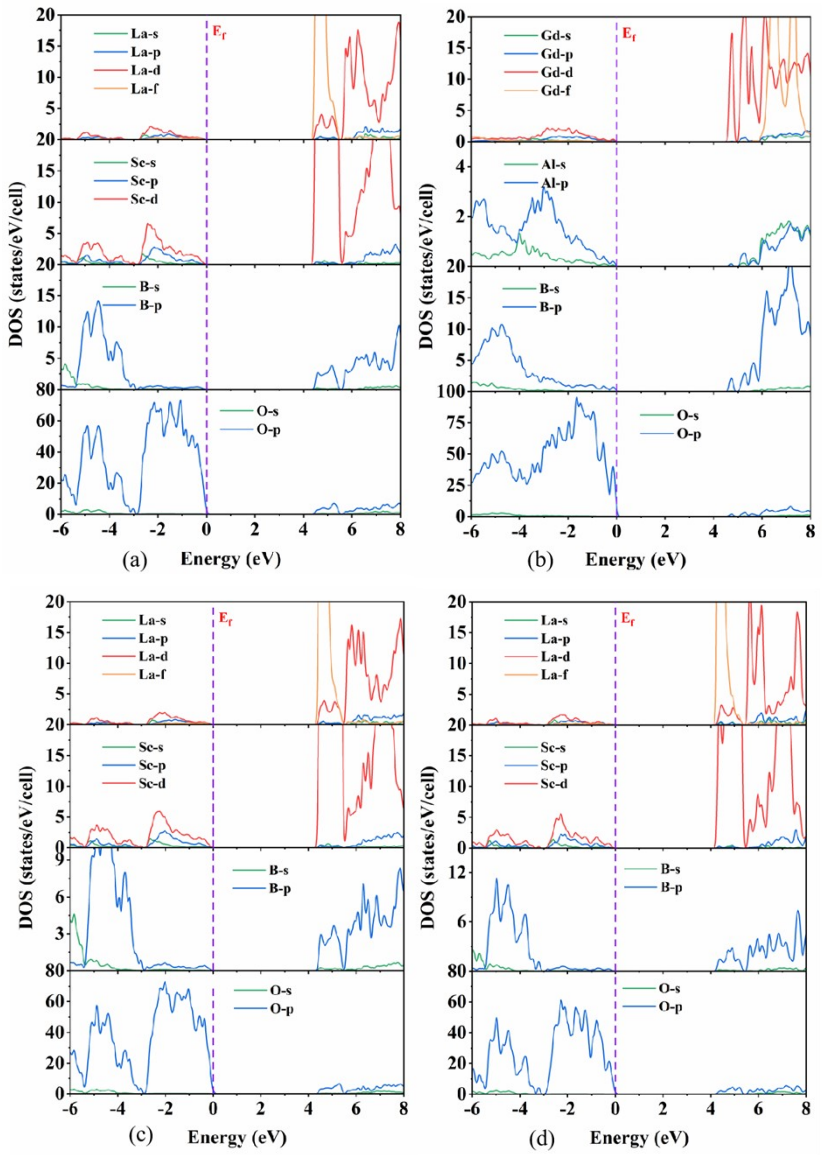

Figure S11. Calculate DOS curvers of the huntite family members: (a) $LaSc_3(BO_3)_4$ (*C*2/*c*), (b) $GdAl_3(BO_3)_4$ (*C*2), (c) $LaSc_3(BO_3)_4$ (*Cc*) and (d) $LaSc_3(BO_3)_4$ (*R*32).

Reference

1 G. M. Sheldrick, *Acta Crystallogr., Sect. A: Found. Adv.*, 2015, **71**, 3–8.

2 O. V. Dolomanov, L. J. Bourhis, R. J. Gildea, J. A. K. Howard and H. Puschmann, *J. Appl. Crystallogr.*, 2009, **42**, 339–341.

3 W. W. Wendlandt and H. G. Hecht, *Reflectance Spectroscopy*; Wiley Interscience: New York, 1966.

4 G. Kortüm, *Reflectance Spectroscopy*; Springer: Berlin, 1969.

5 J. Tauc, R. Grigorovici and A. Vancu, *Phys. Status Solidi B*, 1966, **15**, 627–637.

6 S. J. Clark, M. D. Segall, C. J. Pickard, P. J. Hasnip, M. I. J. Probert, K. Refson and M. C. Payne, Z. Kristallogr. *Cryst. Mater*., 2005, **220**, 567–570.

7 J. P. Perdew, K. Burke and M. Ernzerhof, *Phys. Rev. Lett*., 1996, **77**, 3865–3868.

8 D. R. Hamann, *Phys. Rev. B*, 1989, **40**, 2980–2987.

9 S. F. Li, X. M. Jiang, B. W. Liu, D. Yan, C. S. Lin, H. Y. Zeng and G. C. Guo, *Chem. Mater*., 2017, **29**, 1796–1804.